10400 *Inorg. Chem.* **2010**, *49*, 10400–10408
DOI: 10.1021/ic101184y

Inorganic Chemistry
Article

Electronic Structure of Highly Ruffled Low-Spin Iron(III) Porphyrinates with Electron Withdrawing Heptafluoropropyl Groups at the meso Positions

Akira Tozuka,[‡] Yoshiki Ohgo,[†,‡] Akira Ikezaki,[†] Miyoko Taniguchi,[†] and Mikio Nakamura*[,†,‡]

[†]*Department of Chemistry, School of Medicine, Toho University, Ota-ku, Tokyo 143-8540, Japan, and*
[‡]*Division of Chemistry, Graduate School of Science, Toho University, Funabashi 274-8510, Japan*

Received June 12, 2010

Bis(pyridine)[meso-tetrakis(heptafluoropropyl)porphyrinato]iron(III), $[Fe(THFPrP)Py_2]^+$, was reported to be the low-spin complex that adopts the purest $(d_{xz}, d_{yz})^4(d_{xy})^1$ ground state where the energy gap between the iron d_{xy} and $d_\pi(d_{xz}, d_{yz})$ orbitals is larger than the corresponding energy gaps of any other complexes reported previously (Moore, K. T.; Fletcher, J. T.; Therien, M. J. *J. Am. Chem. Soc.* **1999**, *121*, 5196−5209). Although the highly ruffled porphyrin core expected for this complex contributes to the stabilization of the $(d_{xz}, d_{yz})^4(d_{xy})^1$ ground state, the strongly electron withdrawing C_3F_7 groups at the meso positions should stabilize the $(d_{xy})^2(d_{xz}, d_{yz})^3$ ground state. Thus, we have reexamined the electronic structure of $[Fe(THFPrP)Py_2]^+$ by means of ^{1}H NMR, ^{19}F NMR, and electron paramagnetic resonance (EPR) spectroscopy. The CD_2Cl_2 solution of $[Fe(THFPrP)Py_2]^+$ shows the pyrrole-H signal at −10.25 ppm (298 K) in ^{1}H NMR, the $CF_2(\alpha)$ signal at −74.6 ppm (298 K) in ^{19}F NMR, and the large g_{max} type signal at g = 3.16 (4.2 K) in the EPR. Thus, contrary to the previous report, the complex is unambiguously shown to adopt the $(d_{xy})^2(d_{xz}, d_{yz})^3$ ground state. Comparison of the spectroscopic data of a series of $[Fe(THFPrP)L_2]^+$ with those of the corresponding meso-tetrapropylporphyrin complexes $[Fe(TPrP)L_2]^+$ with various axial ligands (L) has shown that the meso-C_3F_7 groups stabilize the $(d_{xy})^2(d_{xz}, d_{yz})^3$ ground state. Therefore, it is clear that the less common $(d_{xz}, d_{yz})^4(d_{xy})^1$ ground state can be stabilized by the three major factors: (i) axial ligand with low-lying π^* orbitals, (ii) ruffled porphyrin ring, and (iii) electron donating substituent at the meso position.

Introduction

It is well established that low-spin six-coordinate iron(III) porphyrin complexes adopt either the $(d_{xy})^2(d_{xz}, d_{yz})^3$ or the $(d_{xz}, d_{yz})^4(d_{xy})^1$ ground state.[1−14] Considerable studies have revealed that the low-spin complexes tend to adopt the $(d_{xz}, d_{yz})^4(d_{xy})^1$ state if they satisfy either one or both of the following conditions: (i) the complex has axial ligand with low-lying π^* orbitals, and (ii) the complex has ruffled porphyrin ring.[15−21] Thus, the low-spin complexes carrying ^{t}BuNC as axial ligand adopt the $(d_{xz}, d_{yz})^4(d_{xy})^1$ ground state

*To whom correspondence should be addressed. E-mail: mnakamu@med.toho-u.ac.jp.

(1) Safo, M. K.; Gupta, G. P.; Watson, C. T.; Simonis, U.; Walker, F. A.; Scheidt, W. R. *J. Am. Chem. Soc.* **1992**, *114*, 7066–7075.
(2) Safo, M. K.; Walker, F. A.; Raitsimring, A. M.; Walters, W. P.; Dolata, D. P.; Debrunner, P. G.; Scheidt, W. R. *J. Am. Chem. Soc.* **1994**, *116*, 7760–7770.
(3) Cheesman, M. R.; Walker, F. A. *J. Am. Chem. Soc.* **1996**, *118*, 7373–7380.
(4) Walker, F. A.; Nasri, H.; Turowska-Tyrk, I.; Mohanrao, K.; Watson, C. T.; Shokhirev, N. V.; Debrunner, P. G.; Scheidt, W. R. *J. Am. Chem. Soc.* **1996**, *118*, 12109–12118.
(5) Nakamura, M.; Ikeue, T.; Fujii, H.; Yoshimura, T. *J. Am. Chem. Soc.* **1997**, *119*, 6284–6291.
(6) Wołowiec, S.; Latos-Grażyński, L.; Mazzanti, M.; Marchon, J.-C. *Inorg. Chem.* **1997**, *36*, 5761–5771.
(7) Wojaczynski, J.; Latos-Grazynski, L.; Glowiak, T. *Inorg. Chem.* **1997**, *36*, 6299–6306.
(8) Pilard, M.-A.; Guillemot, M.; Toupet, L.; Jordanov, J.; Simonneaux, G. *Inorg. Chem.* **1997**, *36*, 6307–6314.
(9) Wojaczynski, J.; Latos-Grazynski, L.; Toronto, D.; Marchon, J.-C. *Inorg. Chem.* **1998**, *37*, 724–732.
(10) Nakamura, M.; Ikeue, T.; Fujii, H.; Yoshimura, T.; Tajima, K. *Inorg. Chem.* **1998**, *37*, 2405–2414.
(11) Nakamura, M.; Ikeue, T.; Ikezaki, A.; Ohgo, Y.; Fujii, H. *Inorg. Chem.* **1999**, *38*, 3857–3862.
(12) Ikeue, T.; Ohgo, Y.; Saitoh, T.; Nakamura, M.; Fujii, H.; Yokoyama, M. *J. Am. Chem. Soc.* **2000**, *122*, 4068–4076.
(13) Simonneaux, G.; Schünemann, V.; Morice, C.; Carel, L.; Toupet, L.; Winkler, H.; Trautwein, A. X.; Walker, F. A. *J. Am. Chem. Soc.* **2000**, *122*, 4366–4377.
(14) Ikeue, T.; Ohgo, Y.; Saitoh, T.; Yamaguchi, T.; Nakamura, M. *Inorg. Chem.* **2001**, *40*, 3423–3434.
(15) Walker, F. A. Proton NMR and EPR Spectroscopy of Paramagnetic Metalloporphyrins. In *The Porphyrin Handbook*; Kadish, K. M., Smith, K. M., Guilard, R., Eds.; Academic Press: San Diego, CA, 2000; Vol. *5*, pp 81−183.
(16) Walker, F. A. *Inorg. Chem.* **2003**, *42*, 4526–4544.
(17) Walker, F. A. *Chem. Rev.* **2004**, *104*, 589–616.
(18) Nakamura, M. *Coord. Chem. Rev.* **2006**, *250*, 2271–2294.
(19) Nakamura, M.; Ohgo, Y.; Ikezaki, A. *J. Inorg. Biochem.* **2008**, *102*, 433–445.
(20) Ikezaki, A.; Ohgo, Y.; Nakamura, M.. *Coord. Chem. Rev.* **2009**, *253*, 2056–2069.
(21) Nakamura, M.; Ohgo, Y.; Ikezaki, A. Electronic and Magnetic Structures of Iron Porphyrin Complexes. In *Handbook of Porphyrin Science*; Kadish, K. M., Smith, K. M., Guilard, R., Eds.; World Scientific, Singapore, 2010; Vol. *7*, pp 1−146.

Published on Web 10/13/2010

regardless of the nature and positions of peripheral substituents.[13,14,22−28] Conversely, the low-spin complexes carrying imidazole (HIm) almost always adopt the $(d_{xy})^2(d_{xz}, d_{yz})^3$ ground state because HIm is a strong σ donor but weak π acceptor.[12,14]

As for the condition (ii), we have shown that the low-spin complexes having bulky isopropyl groups at the meso positions, $[Fe(T^iPrP)L_2]^{\pm}$, always adopt the $(d_{xz}, d_{yz})^4(d_{xy})^1$ ground state even if the axial ligand is a strong σ donor such as HIm.[12,14] This is because the bulky alkyl groups at the meso position deform the porphyrin ring in a ruffled fashion,[5,6,9,29−36] which makes the interaction between the iron d_{xy} and porphyrin a_{2u} orbital possible and consequently places the d_{xy} orbital above the d_π orbitals.[1,2,37,38]

Electronic effects of peripheral substituents should play some roles in determining the electronic ground state since they affect the energy levels of the porphyrin orbitals, which in turn affects those of the iron 3d orbitals.[39−42] We have found that the sign of the energy gap between the d_{xy} and d_π orbital, $E(d_{xy}) - E(d_\pi)$, is reversed in $[Fe(OETArP)(^tBuNC)_2]^+$ when the meso-aryl (Ar) group is changed from phenyl to 3,5-bis(trifluoromethyl)phenyl group.[22] The result suggests that the electron withdrawing meso-substituent stabilizes the $(d_{xy})^2(d_{xz}, d_{yz})^3$ ground state.

Some years ago, Therien and co-workers reported that $[Fe(THFPrP)Py_2]^+$ adopts the *purest* $(d_{xz}, d_{yz})^4(d_{xy})^1$ ground state on the basis of the electron paramagnetic resonance (EPR) g values at 10 K, that is, $g_x = g_y = 2.07$, $g_z = 1.99$.[43] Here, the *purest* indicates that the energy gap between the d_{xy} and d_π orbitals is much larger than the corresponding energy gaps of any other low-spin complexes reported previously. It is easily expected that the porphyrin ring in $[Fe(THFPrP)Py_2]^+$ is highly ruffled because of the presence of bulky heptafluoropropyl (C_3F_7) groups at the meso positions. Thus, the reason for the purest $(d_{xz}, d_{yz})^4(d_{xy})^1$ ground state in $[Fe(THFPrP)Py_2]^+$ should be ascribed to the extremely ruffled porphyrin structure. However, the C_3F_7 group is a strong electron withdrawing substituent and should contribute to the stabilization of the $(d_{xy})^2(d_{xz}, d_{yz})^3$ ground state.[18,22] Unfortunately, a detailed NMR study has never been done because of the instability of $[Fe(THFPrP)Py_2]^+$; the complex is easily reduced in the presence of excess ligand.[43]

We have been seeking the iron porphyrin complexes with extreme electronic and magnetic properties. Therefore, we are very much interested why $[Fe(THFPrP)Py_2]^+$ adopts the *purest* $(d_{xz}, d_{yz})^4(d_{xy})^1$ ground state in spite of the presence of strong electron withdrawing meso substituents. Here, we report the electronic structure of low-spin $[Fe(THFPrP)Py_2]^+$ as studied by ^1H NMR, ^{13}C NMR, and EPR spectroscopy. We will also compare the electronic structure of a series of $[Fe(THFPrP)L_2]^+$ shown in Figure 1a together with those of the parent $[Fe(TPrP)L_2]^+$ shown in Figure 1b to reveal the electronic effects of meso substituents on the electronic ground state of the low-spin iron(III) porphyrin complexes.

Experimental Section

Instrumentation. UV−vis spectra were recorded for dichloromethane solution on a Shimadzu MultiSpec-1500 spectrophotometer. ^1H NMR spectra were recorded on a JEOL LA300 spectrometer operating at 300.4 MHz for ^1H. Chemical shifts were referenced to the residual peaks of CD_2Cl_2 (δ = 5.32 ppm). Temperature dependent ^1H NMR spectra were taken in CD_2Cl_2 solution in the temperature range 203 to 338 K. Sample tubes were sealed for the high temperature measurement. ^{19}F NMR spectra were recorded on a Bruker Avance II 400 spectrometer operating at 376.5 MHz for ^{19}F. Chemical shifts were referenced to the peak of trifluoromethylbenzene ($\delta = -63.72$ ppm). EPR spectra were recorded at 4.2 K in frozen CH_2Cl_2 solution on a Bruker EMX Plus or E500 spectrometer operating at X band and equipped with an Oxford helium cryostat. To determine g values of the spectra exactly, the observed EPR spectra were simulated by the Bruker WIN-EPR Sim Fonia program. Mass spectra were obtained on a JEOL JMS-600H spectrometer in the FAB-MS mode.

Synthesis. **(THFPrP)H_2** was prepared according to the literature methods. UV−vis, ^1H NMR, and ^{19}F NMR spectra were essentially the same as those reported by DiMagno, Therien and co-workers.[44,45]

Fe(THFPrP)Cl was prepared according to the literature method.[43] UV−vis and ^1H NMR spectra were essentially the same as those reported by Therien and co-workers.[43]

Fe(THFPrP)ClO_4. To a CH_2Cl_2 solution of Fe(THFPrP)Cl (15.0 mg, 1.40×10^{-5} mol) was added a tetrahydrofuran (THF) solution of $AgClO_4$ (2.9 mg, 1.4×10^{-5} mol). The solution was stirred for a minute, and then THF was evaporated. The solid

(22) Ohgo, Y.; Hoshino, A.; Okamura, T.; Uekusa, H.; Hashizume, D.; Ikezaki, A.; Nakamura, M. *Inorg. Chem.* **2007**, *46*, 8193–8207.
(23) Simonneaux, G.; Hindre, F.; Le Plouzennec, M. *Inorg. Chem.* **1989**, *28*, 823–825.
(24) Simonneaux, G.; Kobeissi, M. *J. Chem. Soc., Dalton Trans.* **2001**, 1587–1592.
(25) Cai, S.; Shokhireva, T. K.; Lichtenberger, D. L.; Walker, F. A. *Inorg. Chem.* **2006**, *45*, 3519–3531.
(26) Cai, S.; Lichtenberger, D. L.; Walker, F. A. *Inorg. Chem.* **2005**, *44*, 1890–1903.
(27) Simonneaux, G.; Hindre, F.; Le Plouzennec, M. *Inorg. Chem.* **1989**, *28*, 823–825.
(28) Yatsunyk, L. A.; Walker, F. A. *Inorg. Chem.* **2004**, *43*, 4341–4352.
(29) Scheidt, W. R. In *The Porphyrin Handbook*; Kadish, K. M., Smith, K. M., Guilard, R., Eds.; Academic Press: San Diego, CA, 2000; Vol. *3*, Academic Press, San Diego, 2000, p 49 (Chapter 16).
(30) Ema, T.; Senge, M. O.; Nelson, N. Y.; Ogoshi, H.; Smith, K. M. *Angew. Chem., Int. Ed.* **1994**, *33*, 1879–1881.
(31) Jentzen, W.; Simpson, M. C.; Hobbs, J. D.; Song, X.; Ema, T.; Nelson, N. Y.; Medforth, C. J.; Smith, K. M.; Veyrat, M.; Ramasseul, R.; Marchon, J.-C.; Takeuchi, T.; Goddard, W. A., III.; Shelnutt, J. A. *J. Am. Chem. Soc.* **1995**, *117*, 11085–11097.
(32) Senge, M. O.; Ema, T.; Smith, K. M. *J. Chem. Soc., Chem. Commun.* **1995**, 733–734.
(33) Veyrat, M.; Ramasseul, R.; Marchon, J.-C.; Turowska-Tyrk, I.; Scheidt, W. R. *New J. Chem.* **1995**, *19*, 1199–1202.
(34) Mazzanti, M.; Veyrat, M.; Ramasseul, R.; Marchon, J.-C.; Turowska-Tyrk, H.; Shang, M.; Scheidt, W. R. *Inorg. Chem.* **1996**, *35*, 3733–3734.
(35) Ikeue, T.; Ohgo, Y.; Uchida, A.; Nakamura, M.; Fujii, H.; Yokoyama, M. *Inorg. Chem.* **1999**, *38*, 1276–1281.
(36) Ohgo, Y.; Saitoh, T.; Nakamura, M. *Acta Crystallogr.* **2001**, *C57*, 233–234.
(37) Cheng, R.-J.; Chen, P.-Y.; Lovell, T.; Liu, T.; Noodleman, L.; Case, D. A. *J. Am. Chem. Soc.* **2003**, *125*, 6774–6783.
(38) Conradie, J.; Ghosh, A. *J. Phys. Chem. B.* **2003**, *107*, 6486–6490.
(39) Ochsenbein, P.; Ayougou, K.; Mandon, D.; Fischer, J.; Weiss, R.; Austin, R. N.; Jayaraj, K.; Gold, A.; Terner, J.; Fajer, J. *Angew. Chem., Int. Ed. Engl.* **1994**, *33*, 348–350.
(40) Shokhirev, N. V.; Walker, F. A. *J. Phys. Chem.* **1995**, *99*, 17795–17804.
(41) Murakami, T.; Yamaguchi, K.; Watanabe, Y.; Morishima, I. *Bull. Chem. Soc. Jpn.* **1998**, *71*, 1343–1353.
(42) Ghosh, A.; Halvorsen, I.; Nilsen, H. J.; Steene, E.; Wondimagegn, T.; Lie, R.; van Caemelbecke, E.; Guo, N.; Ou, Z.; Kadish, K. M. *J. Phys. Chem.* **2001**, *105*, 8120–8124.
(43) Moore, K. T.; Fletcher, J. T.; Therien, M. J. *J. Am. Chem. Soc.* **1999**, *121*, 5196–5209.
(44) Goll, J. G.; Moore, K. T.; Ghosh, A.; Therien, M. T. *J. Am. Chem. Soc.* **1996**, *118*, 8344–8354.
(45) DiMagno, S. G.; Williams, R. A.; Therien, M. J. *J. Org. Chem.* **1994**, *59*, 6943–6948.

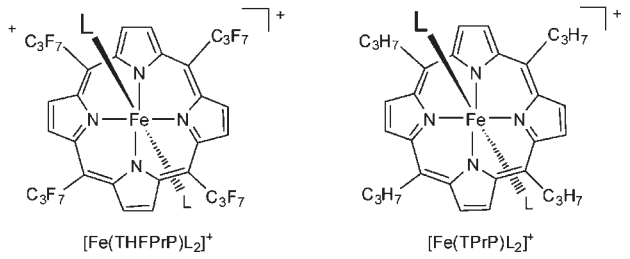

Figure 1. $[Fe(THFPrP)L_2]^+$ and $[Fe(TPrP)L_2]^+$ where L is HIm, 1-MeIm, 2-MeIm, DMAP, 4-MePy, 3-MePy, Py, and ^{t}BuNC.

thus obtained was dissolved into CH_2Cl_2 and then filtered to remove silver chloride. The filtrate, after the addition of pentane, was kept at −78 °C. The dark red solid thus obtained was dried under the argon stream. ***Caution!*** *Perchlorate salts are potentially explosive when heated or shocked. Handle them in milligram quantities with care.* MS (FAB-MS) m/z 1036 ($M^+ - ClO_4$). (calcd 1036). UV−vis (CH_2Cl_2) λ_{max} (log ε) 389 (4.87), 557 (3.93), 655 (3.49) nm. ^{1}H NMR (CD_2Cl_2, 298 K, δ): −26.1 (8H, s, pyrrole-H). ^{19}F NMR (CD_2Cl_2, 298 K, δ): −50.5 (CF_2-α, $W_{1/2}$ = 1100 Hz), −94.2 (CF_2-β, $W_{1/2}$ = 750 Hz), −77.2 (CF_2-γ, $W_{1/2}$ = 28 Hz). EPR (CH_2Cl_2, 4.2 K): g = 5.69, 1.99.

[Fe(THFPrP)L$_2$]ClO$_4$. A series of bis-adducts $[Fe(THFPrP)L_2]ClO_4$ were prepared in an NMR sample tube by the addition of 4 equiv of the ligand (L) to the CD_2Cl_2 solution of Fe(THFPrP)ClO_4. Formation of the bis-adducts was confirmed by the complete disappearance of the broad pyrrole-H signal at −26.1 ppm and the appearance of much sharper pyrrole-H and ligand-H signals of the bis-adducts at more downfield regions with correct ratios in integral intensities.

[Fe(THFPrP)(HIm)$_2$]ClO$_4$. UV−vis (CH_2Cl_2) λ_{max} (log ε) 350 (sh), 406 (4.98), 573 (3.97), 620 (sh). ^{1}H NMR (CD_2Cl_2, 298 K, δ): −14.31 (8H, pyrrole-H), −10.25 (2H, ligand), 6.96 (2H, ligand), 8.17 (2H, broad, ligand). ^{19}F NMR (CD_2Cl_2, 298 K, δ): −82.0 (CF_2-α, $W_{1/2}$ = 1500 Hz), −117.8 (CF_2-β, $W_{1/2}$ = 170 Hz), −81.48 (CF_3-γ, $W_{1/2}$ = 33 Hz). EPR (CH_2Cl_2, 4.2 K): g = 3.40, 3.12, 2.30.

[Fe(THFPrP)(1-MeIm)$_2$]ClO$_4$. UV−vis (CH_2Cl_2) λ_{max} (log ε) 408 (5.05), 576 (3.98), 620 (sh). ^{1}H NMR (CD_2Cl_2, 298 K, δ): −13.96 (8H, s, pyrrole-H), 15.85 (6H, s, ligand-CH_3), −9.74 (2H, ligand), 6.59 (2H, ligand), 5.84(2H, ligand). ^{19}F NMR (CD_2Cl_2, 298 K, δ): −83.4 (CF_2-α, $W_{1/2}$ = 650 Hz), −118.1 (CF_2-β, $W_{1/2}$ = 165 Hz), −81.30 (CF_3-γ, broad t). EPR (CH_2Cl_2, 4.2 K): g = 3.29, 3.02, 2.33.

[Fe(THFPrP)(2-MeIm)$_2$]ClO$_4$. UV−vis (CH_2Cl_2) λ_{max} (log ε) 350 (sh), 408 (4.94), 576 (3.97). ^{1}H NMR (CD_2Cl_2, 298 K): −12.59 (4H, pyrrole-H), −14.43 (2H, pyrrole-H), −15.89 (2H, pyrrole-H), 7.56 (2H, ligand), 14.09 (2H, broad, ligand), 15.18 (6H, ligand-CH_3). ^{19}F NMR (CD_2Cl_2, 298 K, δ): −113.7, −114.6, −118.5 (CF_2-β), −81.1 (CF_3-γ, $W_{1/2}$ = 92 Hz), −80.4 (CF_3-γ, $W_{1/2}$ = 120 Hz).

[Fe(THFPrP)(DMAP)$_2$]ClO$_4$. UV−vis (CH_2Cl_2) λ_{max} (log ε) 341 (4.48), 405 (4.96), 580 (4.00), 696 (sh). ^{1}H NMR (CD_2Cl_2, 298 K): −14.73 (8H, pyrrole-H), 23.64 (12H, ligand-CH_3), −6.09 (4H, ligand-H), 5.95 (4H, ligand-H). ^{19}F NMR (CD_2Cl_2, 298 K, δ): −85.1 (CF_2-α, $W_{1/2}$ = 1000 Hz), −118.6 (CF_2-β, $W_{1/2}$ = 100 Hz), −81.45 (CF_3-γ, broad t). EPR (CH_2Cl_2, 4.2 K): g = 3.42.

[Fe(THFPrP)(4-MePy)$_2$]ClO$_4$. UV−vis (CH_2Cl_2) λ_{max} (log ε) 350 (sh), 406 (4.98), 573 (3.96), 600 (sh). ^{1}H NMR (CD_2Cl_2, 298 K): −18.70 (4H, ligand-H), −11.67 (8H, pyrrole-H), 7.18 (4H, ligand-H), 15.91 (6H, ligand-CH_3). ^{19}F NMR (CD_2Cl_2, 298 K, δ): −78.3 (CF_2-α, $W_{1/2}$ = 1500 Hz), −117.2 (CF_2-β, $W_{1/2}$ = 260 Hz), −80.85 (CF_3-γ, t, J = 10.1 Hz). EPR (CH_2Cl_2, 4.2 K): g = 3.10.

[Fe(THFPrP)(3-MePy)$_2$]ClO$_4$. UV−vis (CH_2Cl_2) λ_{max} (log ε) 350 (sh), 406 (4.94), 573 (3.95), 600 (sh). ^{1}H NMR (CD_2Cl_2, 298 K): −10.94 (8H, pyrrole-H), −22.59 (2H, ligand-H), −17.46 (2H, ligand-H), 1.54 (2H, ligand-H), 7.00 (2H, ligand-H), 1.54 (6H, ligand-CH_3). ^{19}F NMR (CD_2Cl_2, 298 K, δ): −77.3 (CF_2-α, $W_{1/2}$ = 1100 Hz), −116.8 (CF_2-β, $W_{1/2}$ = 240 Hz), −80.67 (CF_3-γ, broad t, J = 9.2 Hz).

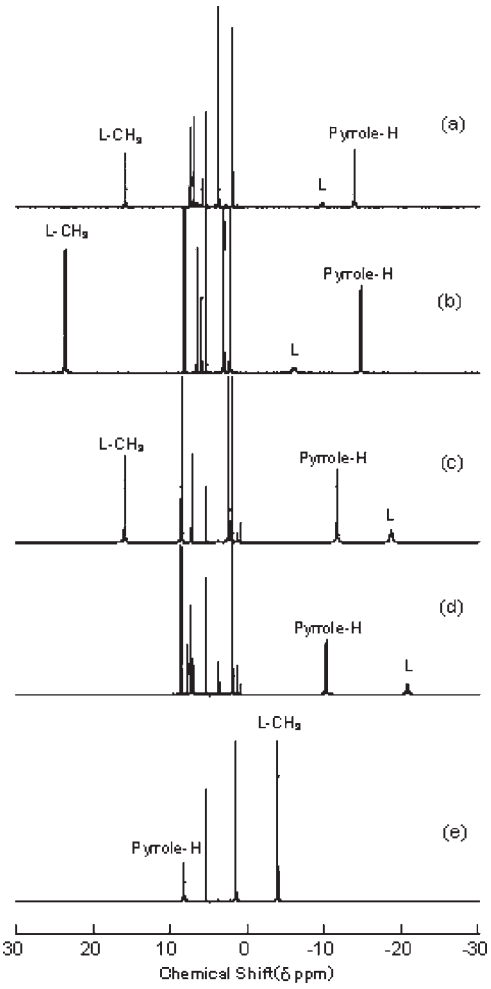

Figure 2. ^{1}H NMR spectra of $[Fe(THFPrP)L_2]ClO_4$ taken in CD_2Cl_2 solution at 298 K where axial ligand is (a) 1-MeIm, (b) DMAP, (c) 4-MePy, (d) Py, and (e) ^{t}BuNC. Signals signified as L and L-CH_3 correspond to the ligand ring proton and ligand methyl protons, respectively.

[Fe(THFPrP)Py$_2$]ClO$_4$. UV−vis(CH_2Cl_2) λ_{max}(log ε) 350 (sh), 406 (4.96), 573 (3.96), 600 (sh). ^{1}H NMR (CD_2Cl_2, 298 K): −10.25 (8H, s, pyrrole-H), −20.80 (2H, ligand-2,6-H), 7.06 (4H, liand-3, 5-H), 1.33 (2H, ligand-4H). ^{19}F NMR (CD_2Cl_2, 298 K, δ): −74.6 (CF_2-α, $W_{1/2}$ = 1500 Hz), −116.5 (CF_2-β, $W_{1/2}$ = 300 Hz), −80.60 (CF_3-γ, t, J = 9.9 Hz). EPR (CH_2Cl_2, 4.2 K): g = 3.16.

[Fe(THFPrP)(^{t}BuNC)$_2$]ClO$_4$. UV−vis (CH_2Cl_2) λ_{max} (log ε) 351 (4.48), 409 (4.92), 584 (4.11). ^{1}H NMR (CD_2Cl_2, 298 K): 8.22 (8H, s, pyrrole-H), −3.97 (18H, ligand-CH_3). ^{19}F NMR (CD_2Cl_2, 298 K, δ): −103.5 (CF_2-β, $W_{1/2}$ = 640 Hz), −77.96 (CF_3-γ, 18 Hz). EPR (CH_2Cl_2, 4.2 K): g = 2.35, 1.84.

Determination of the Rate Constants for Ligand Rotation. Line shape analysis for the pyrrole-H signals of $[Fe(THFPrP)(2\text{-}MeIm)_2]^+$ was performed using gNMR(Ver. 5) software purchased from Adept Scientific, Amor Way, Letchworth Herts SG6 1ZA, U.K. The chemical shifts of the pyrrole-H in the temperature range where the line shape changes were determined by the extrapolation from the low temperature data where the rotation is slow on the ^{1}H NMR time scale. The half-height width of each signal was kept constant, that is, 80 Hz, throughout the calculation.

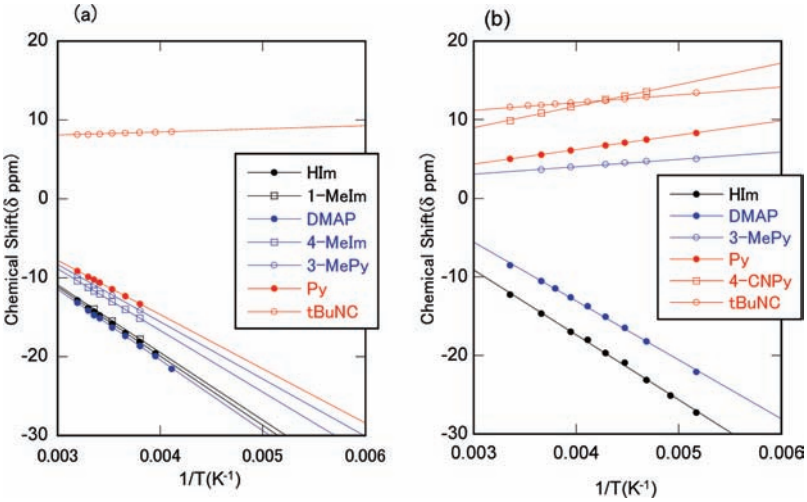

Figure 3. Curie plots of the pyrrole-H signals in (a) $[Fe(THFPrP)L_2]^+$ and (b) $[Fe(TPrP)L_2]^+$.

Results

^{1}H NMR Spectra. Figure 2 shows the ^{1}H NMR spectra of a series of $[Fe(THFPrP)L_2]^+$ taken in CD_2Cl_2 solution at 298 K. While the complexes carrying nitrogen bases exhibited the pyrrole-H signals at −10.25 to −14.73 ppm, the ^{t}BuNC complex showed the signal at +8.22 ppm. The ^{1}H NMR spectra in Figure 2 also indicate that the rate for ligand dissociation is slow on the ^{1}H NMR time scale at 298 K since the signals of the free and coordinating ligands were observed separately.[46] Figure 3a shows the Curie plots of the pyrrole-H signals of all the low-spin complexes examined in this study. The complexes carrying nitrogen bases showed good straight lines with negative slopes while the ^{t}BuNC complex exhibited the straight line with a small positive slope. For comparison, the Curie plots of the pyrrole-H signals of analogous $[Fe(TPrP)L_2]^+$ are given in Figure 3b.[12,14] Figure 4 shows the temperature dependent ^{1}H NMR spectra of $[Fe(THFPrP)(Py)_2]^+$. As the temperature was lowered, the pyrrole and coordinating pyridine signals broadened and split into several lines. At 203 K, a major pyrrole signal was observed at −24.1 ppm together with several weak signals ranging from −15 to −34 ppm. Similarly, a major signal for the pyridine-3,5-H was observed at 14.2 ppm together with some weak signals at 10.9, 11.1, and 11.5 ppm. Other low-spin complexes examined in this study exhibited the similar spectral change as the temperature was lowered. Figure 5 shows the temperature dependent pyrrole-H signals of $[Fe(THFPrP)(2\text{-}MeIm)_2]^+$ together with the calculated ones. At 303 K, the pyrrole-H gave three signals at −12.0, −13.8, and −15.2 ppm with relative intensities of 2:1:1. These signals broadened with temperature and gave a symmetrical signal above 333 K. Table 1 lists the ^{1}H NMR chemical shifts of a series of $[Fe(THFPrP)L_2]^+$ and $[Fe(TPrP)L_2]^+$ determined at 298 K in CD_2Cl_2 solutions.

^{19}F NMR Spectra. Figure 6 shows the ^{19}F NMR spectra of $[Fe(THFPrP)L_2]^+$ taken in CD_2Cl_2 solution at 298 K. While the $CF_3(\gamma)$ showed either a singlet with half-height widths of about 30 Hz or a triplet with J = about 10 Hz, the $CF_2(\beta)$ showed much broader singlet at more upfield positions; the half-height widths were 100 to 300 Hz. The $CF_2(\alpha)$ commonly showed very broad signal;

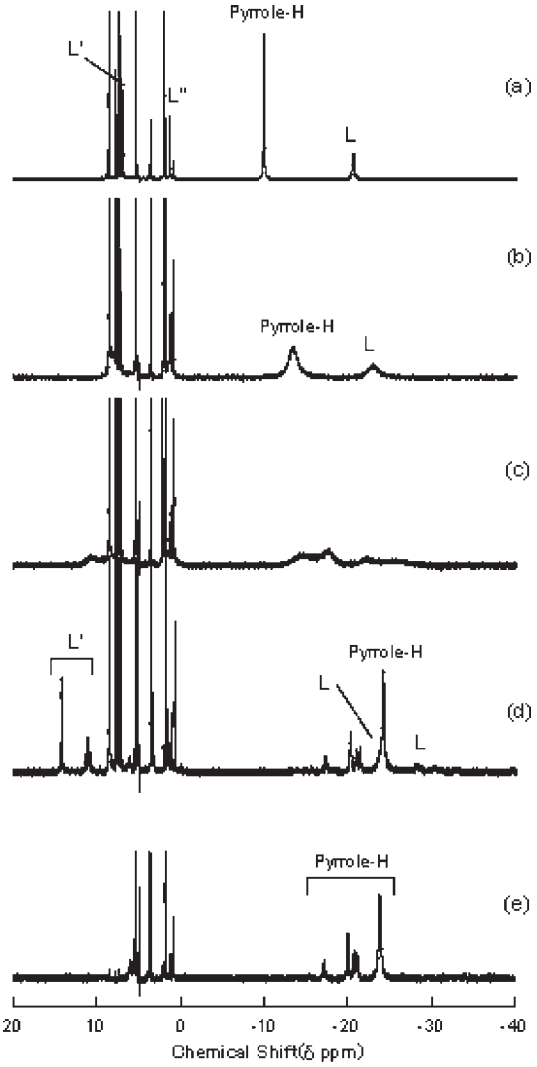

Figure 4. Temperature dependent ^{1}H NMR spectra of $[Fe(THFPrP)Py_2]^+$ taken in CD_2Cl_2 solution: (a) 303 K, (b) 263 K, (c) 243 K, (d) 203 K, and (e) 203 K with pyridine-d_5. L, L′, and L″ indicate the 2,6-H, 3,5-H, and 4-H of the coordinating pyridine protons, respectively.

(46) Nakamura, M. *Inorg. Chim. Acta* **1989**, *161*, 73–80.

the half-height widths reached as much as 1500 Hz. The $CF_2(\alpha)$ of the ^{t}BuNC complex exhibited an extremely broad signal around −27.4 ppm. The half-height width was estimated to be about 4000 Hz. The ^{19}F NMR chemical shifts of these complexes are also listed in Table 1. The isotropic shift (δ_{iso}) of each ^{19}F signal in $[Fe(THFPrP)L_2]^+$, which is the sum of contact and dipolar shifts (δ_{con} and δ_{dia}, respectively), was calculated by the subtraction of the chemical shift (δ_{dia}) of diamagnetic $[Fe(THFPrP)Py_2]$ from the observed one (δ_{obs}) according to eq 1; the $CF_2(\alpha)$, $CF_2(\beta)$ and $CF_3(\gamma)$ chemical shifts of diamagnetic $[Fe(THFPrP)Py_2]$ were reported to be −86.2, −119.37, and −79.97 ppm, respectively.[43] These isotropic shifts are also given in Table 1 in italics.

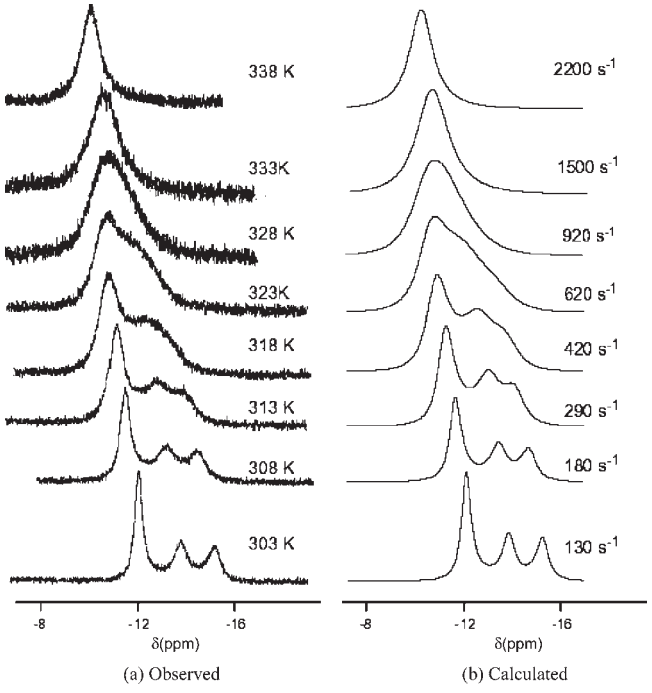

Figure 5. (a) Temperature dependent pyrrole-H signals of $[Fe(THFPrP)(2\text{-MeIm})_2]^+$ in CD_2Cl_2 solution. (b) Calculated spectra.

$$\delta_{iso} = \delta_{con} + \delta_{dip} = \delta_{obs} - \delta_{dia} \quad (1)$$

Figure 7a shows the correlation of the chemical shifts between pyrrole-H and $CF_2(\alpha)$ in $[Fe(THFPrP)L_2]^+$. For comparison, the correlation of the chemical shifts between pyrrole-H and $CH_2(\alpha)$ in $[Fe(TPrP)L_2]$ is given in Figure 7b. In both cases, the correlation curves exhibit positive slopes.

EPR Spectra. Figure 8 shows the EPR spectra of a series of $[Fe(THFPrP)L_2]^+$ taken in frozen CH_2Cl_2 solution at 4.2 K. The g values were determined by the computer simulation of the observed spectra. They are listed in Table 2 together with those of corresponding $[Fe(TPrP)L_2]^+$.

Discussion

Stable Conformations of $[Fe(THFPrP)L_2]^+$. Temperature dependent ^{1}H NMR spectra of $[Fe(THFPrP)(Py)_2]^+$ shown in Figure 4 indicate that some dynamic processes are slowed down on the ^{1}H NMR time scale as the temperature is lowered. There are four possible dynamic processes in this complex; (a) ligand exchange between free and coordinating axial ligand,[46] (b) inversion of the

Table 1. ^{1}H and ^{19}F NMR Chemical Shifts[a] of (a) $[Fe(THFPrP)L_2]^+$ and (b) $[Fe(TPrP)L_2]^+$ [b]

	^{1}H NMR					^{19}F NMR[c] (^{1}H NMR[d])		
L	pyrrole-H	ligand[e]				$CF_2(\alpha)$	$CF_2(\beta)$	$CF_3(\gamma)$
				(a) $[Fe(THFPrP)L_2]^+$				
HIm	−14.31		−10.25	8.17(br)	6.94	−82.0	−117.8	−81.48
						4.2	*1.6*	*-1.51*
1-MeIm	−13.96	(15.85)	−9.74	6.59(br)	5.84	−83.4	−118.1	−81.30
						2.8	*1.3*	*-1.33*
DMAP	−14.73	(23.64)	−6.09	5.95		−85.1	−118.6	−81.45
						1.1	*0.8*	*-1.48*
4-MePy	−11.67	(15.91)	−18.70	7.18		−78.3	−117.2	−80.85
						7.9	*2.1*	*-0.88*
3-MePy	−10.94	(0.74)	−22.59	7.00	1.54	−77.3	−116.8	−80.67
			−17.46			*8.9*	*2.6*	*-0.70*
Py	−10.25		−20.80	7.06	1.33	−74.6	−116.5	−80.60
						11.6	*2.9*	*-0.63*
tBuNC	+8.22	(−3.95)				*-27.4*	−112.0	−79.27
						58.8	*7.4*	*+0.70*
				(b) $[Fe(TPrP)L_2]^+$				
HIm	−12.20	−10.77	11.47	5.82	4.30	(5.08)	(−0.03)	(0.10)
1-MeIm	−11.21	(12.85)	4.44	3.67	3.67	(7.15)	(2.62)	(0.07)
DMAP	−8.53	(12.43)	−14.83	4.62		(11.60)	(0.31)	(−0.04)
3-MePy	3.37	(−1.76)[f]	−23.09[f]	−1.09[f]	0.17[f]	(37.38)	(1.37)	(−0.29)
			−23.59[f]					
Py	5.01		−23.14[f]	−1.81[f]	0.17[f]	(41.15)	(1.22)	(−0.38)
4-CNPy	9.89		−22.57[g]	−4.00[g]		(63.01)	(1.22)	(−0.38)
^{t}BuNC	11.60	−1.53				(95.20)	(−2.15)	(2.17)

[a] Determined in CD_2Cl_2 solution at 298 K. [b] Ikeue et al. refs 12, 14. [c] Numbers written in italics are the isotropic shifts. [d] Numbers in parentheses are the chemical shifts of the propyl-H signals. [e] Numbers in parentheses are the chemical shifts of the methyl signals in the axial ligands. [f] Extrapolated from the low temperature data. [g] Data at 253 K.

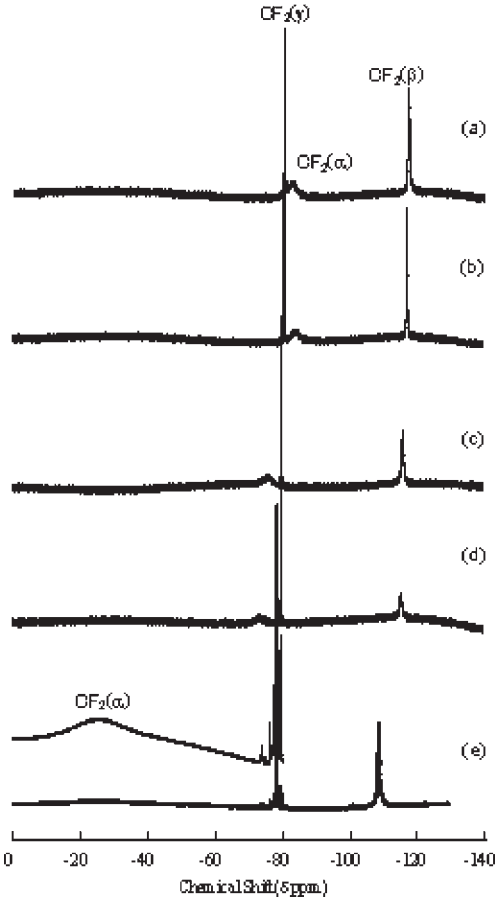

Figure 6. ^{19}F NMR spectra of $[Fe(THFPrP)L_2]^+$ taken in CD_2Cl_2 solution at 298 K where axial ligand is (a) 1-MeIm, (b) DMAP, (c) 4-MePy, (d) Py, and (e) ^{t}BuNC.

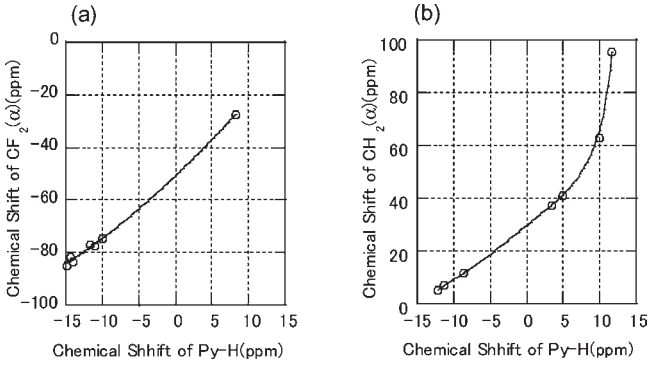

Figure 7. Correlation of the chemical shifts (a) between $CF_2(\alpha)$ and pyrrole-H in $[Fe(THFPrP)L_2]^+$, and (b) between $CH_2(\alpha)$ and pyrrole-H in $[Fe(TPrP)L_2]^+$.

ruffled porphyrin ring,[43] (c) rotation of the axial ligand around the Fe−N bond,[10,47−54] and (d) rotation of the meso-C_3F_7 group around the C_{meso}-$CF_2(\alpha)$ bond. In the present case, the process (a) must be slow on the ^{1}H NMR time scale since the signals for the free and coordinating

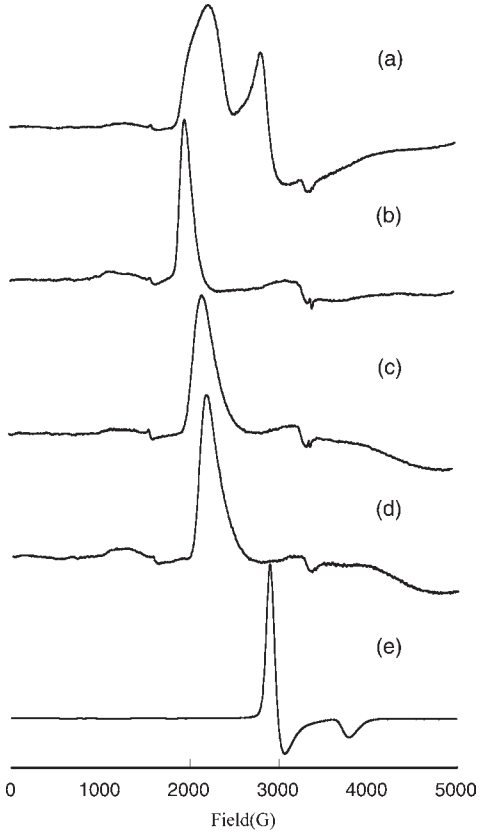

Figure 8. EPR spectra of a series of $[Fe(THFPrP)L_2]^+$ taken in frozen CH_2Cl_2 solution at 4.2 K where L is (a) 1-MeIm, (b) DMAP, (c) 4-MePy, (d) Py, and (e) ^{t}BuNC.

Table 2. EPR g Values Determined in Frozen CH_2Cl_2 Solution at 4.2 K

L	g_1	g_2	g_3
	$[Fe(THFPrP)L_2]^{+a}$		
HIm	3.12	2.30	(0.99)[b]
	3.40		
1-MeIm	3.02	2.33	
	3.29		
DMAP	3.42		
4-MePy	3.10		
Py	3.16		
4-CNPy	n.d.		
^{t}BuNC	2.35	2.35	1.84
	$[Fe(TPrP)L_2]^{+c}$		
HIm	2.90	2.35	(1.45)[b]
1-MeIm	n.d.		
DMAP	3.10	2.10	(1.41)[b]
4-MePy	n.d.		
Py	2.55	2.55	
4-CNPy	2.46	2.46	1.68
^{t}BuNC	2.16	2.16	1.95

[a] This work. [b] Data in parenthesis are obtained from $g_1^2 + g_2^2 + g_3^2 = 16$. [c] Ikeue et al. refs 12, 14.

(47) Nakamura, M.; Groves, J. T. *Tetrahedron* **1988**, *44*, 3225–3230.
(48) The stable conformation of $[Fe(TMP)(2\text{-MeIm})_2]^+$ proposed in refs 46, 47 was revised later.[49,50]
(49) Nakamura, M.; Nakamura, N. *Chem. Lett.* **1991**, *20*, 1885–1888.
(50) Walker, F. A.; Simonis, U. *J. Am. Chem. Soc.* **1991**, *113*, 8652–8657.
(51) Nakamura, M.; Ikeue, T.; Neya, S.; Funasaki, N.; Nakamura, N. *Inorg. Chem.* **1996**, *35*, 3731–3732.
(52) Shokhirev, N. V.; Shokhireva, T. K.; Polam, J. R.; Watson, C. T.; Raffii, K.; Simonis, U.; Walker, F. A. *J. Phys. Chem. A.* **1997**, *101*, 2778–2786.
(53) Momot, K. I.; Walker, F. A. *J. Phys. Chem. A.* **1998**, *102*, 10682–10688.
(54) Ikezaki, A.; Takahashi, M.; Nakamura, M. *Angew. Chem., Int. Ed.* **2009**, *48*, 1–5.

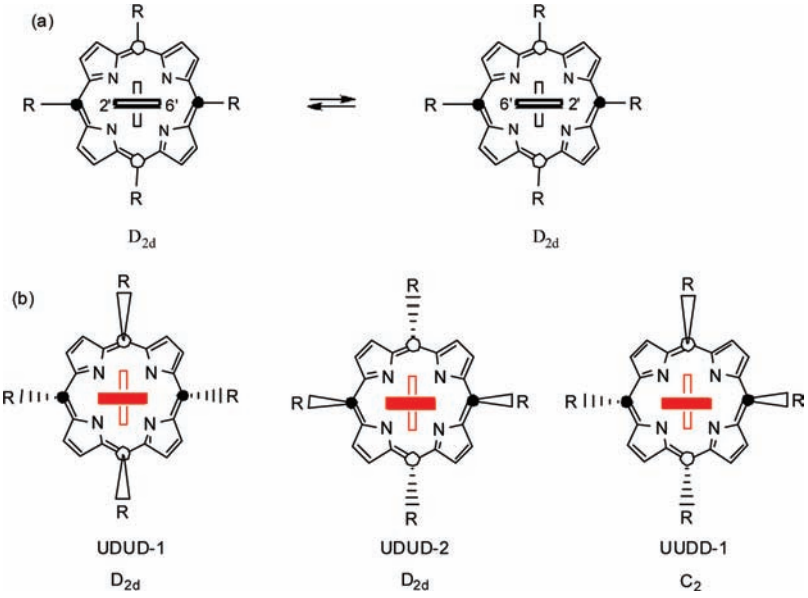

Figure 9. Dynamic processes in highly ruffled $[Fe(THFPrP)(4\text{-}MePy)_2]^+$. The filled and open circles at the meso carbon atoms indicate that they deviate from the mean porphyrin plane upward(U) and downward(D), respectively. (a) Rotation of axial ligand in ruffled porphyrin framework. Note that all the pyrrole-H, pyridine-2,6-H, and pyridine-3,5-H are equivalent even if the process is frozen. (b) Rotation of the meso-C_3F_7 groups about the $C_{meso}-CH_2(\alpha)$ single bonds. Only three of the six possible conformers expected for $[Fe(THFPrP)Py_2]^+$, UDUD-1, UDUD-2, and UUDD-1, are given. While these conformers commonly exhibit one signal for the pyridine-CH_3, they show one, one, and four signals for the pyrrole-H, respectively.

ligand were observed separately as shown in Figure 2. The process (b) is expected to be slow because of the presence of bulky substituents at the meso position.[55] In fact, Fe(THFPrP)Cl exhibits two pyrrole-H signals even at ambient temperature.[43] The process (c) is known to be slow in highly ruffled porphyrin complexes carrying sterically hindered axial ligands such as $[Fe(T\textit{i}PrP)(2\text{-}MeIm)_2]^+$ and $[Fe(TMP)(2\text{-}MeBzIm)_2]^+$.[49,51] In these complexes, the planar ligands are fixed along the diagonal $C_{meso}-Fe-C_{meso}$ axes in a mutually perpendicular fashion.[47−50] Thus, the axial Py ligand in $[Fe(THFPrP)(Py)_2]^+$ should be placed similarly along the diagonal $C_{meso}-Fe-C_{meso}$ axes. The perpendicular alignment of the pyridine ligand was further confirmed by the large g_{max} type EPR spectrum as shown in Figure 8d. It should be noted, however, that the rate for ligand rotation causes no effect on the temperature dependent line shapes of the pyrrole-H and ligand-H signals as far as the axial ligand is symmetrical such as Py or 4-MePy as shown in Figure 9a.

The splitting of the pyrrole-H and ligand-H signals can be explained only when the process (d) is hindered. In fact, some examples are known where the pyrrole-H signal splits into several lines because of the hindered rotation around the $C_{meso}-CH_2(\alpha)$ bond.[32,56,57] In the present case, there are six possible conformers depending on the orientation of the meso-C_3F_7 groups. They are UUUU, UUUD-1, UUUD-2, UDUD-1, UDUD-2, and UUDD, where U(up) and D(down) indicate the direction of $CF_2(\beta)$ group relative to the porphyrin plane. These conformers should give totally 16 signals for the pyrrole-H, 9 signals for the pyridine-4-H, 12 signals for the pyridine-2,6-H and pyridine-3,5-H. In Figure 9b are shown three of the six possible conformers, UDUD-1, UDUD-2, and UUDD-1. Close inspection of the ^1H NMR spectrum at 203 K in Figure 4 reveals that the major conformer is the one that exhibits a single signal for the pyrrole-H. Thus, either UDUD-1 or UDUD-2 should exist as a major conformer because both of these conformers satisfy the spectral conditions mentioned above. The ^1H NMR spectra of all the other complexes examined in this study have exhibited the similar spectral change.

Barriers to Rotation of Axial Ligands in $[Fe(THFPrP)L_2]^+$. As mentioned, the ligand rotation process cannot be observed from the ^1H NMR spectra as far as the complex has symmetrical ligands such as Py and 4-MePy. To reveal the rate for ligand rotation in $[Fe(THFPrP)(Py)_2]^+$, the ^1H NMR spectra of the complex carrying unsymmetrical pyridine ligand $[Fe(THFPrP)(3\text{-}MePy)_2]^+$ have been taken at various temperatures. As shown in the Supporting Information, Figure S1, the pyrrole-H exhibited a single sharp signal at 298 K. Thus, the rotation of the unsubstituted pyridine ligand should be fast on the ^1H NMR time scale. It should be noted that the rotation of the analogous 3-chloropyridine ligand in $[Co(T^tBuP)(3\text{-}ClPy)_2]^+$ is hindered even at ambient temperature as is revealed from the four separate signals of the pyrrole-H. The result should be ascribed to the extremely ruffled porphyrin structure in $[Co(T^tBuP)(3\text{-}ClPy)_2]^+$; the axial ligand is fixed in the cavity caused by the highly ruffled porphyrin core.[58]

In contrast to the 3-MePy complex, the corresponding complex carrying sterically much hindered 2-MeIm showed three separate pyrrole-H signals at −12.47, −14.43, and −15.76 ppm with integral intensity ratios 2:1:1 at 298 K as shown in Figure 5a. As the temperature was raised, these

(55) Ikezaki, A.; Nakamura, M. *Chem. Lett.* **2005**, *34*, 1046–1047.
(56) Ikeue, T.; Ohgo, Y.; Uchida, A.; Nakamura, M.; Fujii, H.; Yokoyama, M. *Inorg. Chem.* **1999**, *38*, 1276–1281.
(57) For a review of the hindered rotation about the C−C single bond, see: Oki, M. In *Application of Dynamic NMR Spectroscopy to Organic Chemistry*; Marchand,A. P., Ed.; Methods in Stereochemical Analysis; VCH: Deerfield Beach, FL, 1985; Vol. *4*, p 423.
(58) Medforth, C. J.; Muzzi, C. M.; Shea, K. M.; Smith, K. M.; Abraham, R. J.; Jia, S.; Shelnutt, J. A. *J. Chem. Soc., Perkin Trans. 2* **1997**, 833–837.

signals broadened and became a symmetrical signal above 333 K. Figures 5b exhibits the best-fit calculated spectra corresponding to the observed ones, from which the rate constants for the ligand rotation were determined as follows:130 s^{-1} (303 K), 180 s^{-1} (308 K), 290 s^{-1} (313 K), 420 s^{-1} (318 K), 620 s^{-1} (323 K), 920 s^{-1} (328 K), 1500 s^{-1} (333 K), and 2200 s^{-1} (338 K). Thus, the activation enthalpy ($\Delta H^{\ddagger}$) and entropy($\Delta S^{\ddagger}$) for the ligand rotation are estimated to be 66.8 kJ mol^{-1} and 15.4 J K^{-1} mol^{-1}, respectively. The result contrasts to the case of $[Fe(TPrP)(2\text{-}MeIm)_2]^+$ which shows a sharp pyrrole-H signal at 298 K.[12] The high barrier to ligand rotation in $[Fe(THFPrP)(2\text{-}MeIm)_2]^+$ indicates that the porphyrin core in $[Fe(THFPrP)(2\text{-}MeIm)_2]^+$ is much more ruffled than that in $[Fe(TPrP)(2\text{-}MeIm)_2]^+$.

Determination of Electronic Structure of Low-Spin $[Fe(THFPrP)L_2]^+$. (i) ^{1}H NMR Spectroscopy. The ^{1}H NMR spectroscopy is a powerful method to elucidate the electronic structure of low-spin iron(III) porphyrin complexes because we can determine which d orbital is half-occupied on the basis of the isotropically shifted proton signals.[15−21] If the low-spin complex adopts the $(d_{xy})^2(d_{xz}, d_{yz})^3$ ground state, the half-occupied iron $d_\pi(d_{xz}, d_{yz})$ orbital interacts with the fully occupied porphyrin $3e_g$ orbital, which induces sizable spin densities on the pyrrole β carbon atoms. The contact shift (δ_{con}) of the pyrrole-H signal is given by eq 2, where K_1 is a positive constant, T is an absolute temperature, and ρ is a spin density on the pyrrole β carbon atom. Thus, the contact shift of the pyrrole-H signal should be negative (upfield shift).

$$\delta_{con} = K_1\rho/T \qquad (2)$$

In addition to the contact shift, the dipolar shift (δ_{dip}) given by eq 3 for the complexes with axial symmetry should also be negative (upfield shift) for the pyrrole-H signal.

$$\delta_{dip} = K_2(g_\parallel{}^2 - g_\perp{}^2)[(3\cos^2\theta - 1)/r^3)]/T \qquad (3)$$

This is because the $g_\parallel{}^2 - g_\perp{}^2$ term is positive in the $(d_{xy})^2(d_{xz}, d_{yz})^3$ type low-spin complexes, while the geometric factor $(3\cos^2\theta - 1)/r^3$ is negative for the pyrrole-H. As a result of the contact and dipolar shifts, the pyrrole-H signal appears at the upfield position and shows negative slope in the Curie plots.

The situation is different in the low-spin complexes adopting the $(d_{xz}, d_{yz})^4(d_{xy})^1$ ground state. The major interaction occurs between the half-occupied iron d_{xy} and porphyrin a_{2u} orbital in the ruffled porphyrin framework; the $(d_{xz}, d_{yz})^4(d_{xy})^1$ type low-spin complexes generally have a highly ruffled porphyrin core.[15−21] Since the a_{2u} orbital has zero coefficient on the pyrrole β carbon atoms, the upfield shift of the pyrrole-H signal due to the contact contribution should be quite small. In contrast to the case of the $(d_{xy})^2(d_{xz}, d_{yz})^3$ type complexes, the dipolar shift of the pyrrole-H signal given by eq 3 should be positive (downfield shift) because both the $g_\parallel{}^2 - g_\perp{}^2$ term and geometric factor are negative. It should be noted that the dipolar contribution to the isotropic shift is much smaller in the $(d_{xz}, d_{yz})^4(d_{xy})^1$ type than in the $(d_{xy})^2(d_{xz}, d_{yz})^3$ type complexes because of the smaller $g_\parallel{}^2 - g_\perp{}^2$ term in the former complexes.[15] Thus, the pyrrole-H signal should appear close to the diamagnetic position and moves either downfield or upfield linearly with a small slope with the inverse temperature ($1/T$).

The pyrrole-H signals of the HIm, 1-MeIm, DMAP, 4-MePy, 3-MePy, and Py complexes appeared at −14.31 −13.96, −14.73, −11.67, −10.94, and −10.25 ppm, respectively, at 298 K. Correspondingly, all these complexes exhibited fairly large negative slopes as shown in Figure 3a; they are -8.78×10^3, -8.58×10^3, -8.99×10^3, -7.83×10^3, -7.27×10^3, and -6.75×10^3 ppm K, respectively. Thus, the chemical shifts and the Curie slopes of the pyrrole-H signals in these complexes suggest that they adopt the $(d_{xy})^2(d_{xz}, d_{yz})^3$ ground state in the NMR temperature range 313−173 K. In the case of the ^{t}BuNC complex, the chemical shift and the Curie slope of the pyrrole-H signal were +8.20 ppm (298 K) and $+0.40 \times 10^3$ ppm K, respectively. The presence of the pyrrole-H signal close to the diamagnetic position together with a small positive slope of the Curie plots suggest that the ^{t}BuNC complex adopts the $(d_{xz}, d_{yz})^4(d_{xy})^1$ ground state as most of the other ^{t}BuNC complexes reported previously.[4,13,14,22−28,59,60]

(ii) ^{19}F NMR Spectroscopy. The relationship between the ^{19}F NMR chemical shifts and the electronic structure of iron(III) porphyrin complexes is not well understood.[61−63] The data in Table 1a indicate that the $CF_2(\alpha)$ signal shows a small downfield shift from −82.0 to −74.6 ppm as the axial ligand changes from HIm to Py. Only $[Fe(THFPrP)(^tBuNC)_2]^+$ exhibits a very broad $CF_2(\alpha)$ signal at a fairly downfield position (δ = −27.4 ppm), indicative of the $(d_{xz}, d_{yz})^4(d_{xy})^1$ ground state. Figure 7a shows the correlation of the chemical shifts between $CF_2(\alpha)$ and pyrrole-H in $[Fe(THFPrP)L_2]^+$. Corresponding to the downfield shift of the pyrrole-H signal, the $CF_2(\alpha)$ signal also moves downfield. Since the downfield shift of the pyrrole-H signal in low-spin iron(III) porphyrin complexes is directly connected with the increase in population of

$$(d_{xy})^2(d_{xz}, d_{yz})^3 \rightleftarrows (d_{xz}, d_{yz})^4(d_{xy})^1 \qquad (4)$$

the spin-isomer that adopts the $(d_{xz}, d_{yz})^4(d_{xy})^1$ ground state as shown in eq 4, the correlation given in Figure 7a clearly indicates that the $CF_2(\alpha)$ signal can also be a good probe to elucidate the electronic structure of low-spin iron(III) porphyrin complexes.

(iii) EPR Spectroscopy. The EPR spectra given in Figure 8 and g values listed in Table 2 suggest that all the complexes except for $[Fe(THFPrP)(^tBuNC)_2]^+$ adopt the $(d_{xy})^2(d_{xz}, d_{yz})^3$ ground state. Both the HIm and 1-MeIm complexes exhibited the rhombic type signals together with much weaker large g_{max} type signal. The results suggest that the frozen CH_2Cl_2 solutions of these complexes contain two conformers at 4.2 K; one has parallel aligned axial ligands and shows the rhombic type spectrum while the other has perpendicularly aligned

(59) Ohgo, Y.; Neya, S.; Uekusa, H.; Nakamura, M. *Chem. Commun.* **2006**, 4590–4592.
(60) Nakamura, K.; Ikezaki, A.; Ohgo, Y.; Ikeue, T.; Neya, S.; Nakamura, M. *Inorg. Chem.* **2008**, *47*, 10299–10307.
(61) Birnbaum, E. R.; Hodge, J. A.; Grinstaff, M. W.; Schaefer, W. P.; Henling, L.; Labinger, J. A.; Bercaw, J. E.; Gray, H. B. *Inorg. Chem.* **1995**, *34*, 3625–3632.
(62) Grinstaff, M. W.; Hill, M. G.; Birnbaum, E. R.; Schaefer, W. P.; Labinger, J. A.; Gray, H. B. *Inorg. Chem.* **1995**, *34*, 4896–4902.
(63) Cai, S.; Licoccia, S.; D'Ottavi, C.; Paolesse, R.; Nardis, S.; Bulach, V.; Zimmer, B.; Shokhireva, T. K.; Walker, F. A. *Inorg. Chim. Acta* **2002**, *339*, 171–178.
(64) Yatsunyk, L.; Walker, F. A. *Inorg. Chim. Acta* **2002**, *337*, 266–274.

axial ligands and gives large g_{max} type spectrum.[64,65] Direct observation of the conformational isomers by EPR spectroscopy indicates that the difference in free energy between two conformers ($\Delta G°$) are less than 200 J/mol at 4.2 K in the HIm and 1-MeIm complexes; the value is estimated under the assumption that the two isomers are in the equilibrium state with K less than 300.[66] If we assume K to be 10, then the $\Delta G°$ decreases to 80 J/mol. In contrast, the DMAP, 4-MePy, and Py complexes exhibit only the large g_{max} type signals, suggesting that these complexes exist as a single isomer with perpendicularly aligned axial ligands. The presence of a single conformational isomer in these complexes should be ascribed to the bulkier six-membered pyridine ligands as compared with the five-membered HIm and 1-MeIm ligands. This is because the bulky axial ligands suffer much larger steric repulsion from the ruffled porphyrin core if they take parallel conformation rather than the perpendicular one. Only the ^{t}BuNC complex exhibits the axial type spectrum with $g_\perp = 2.35$ and $g_\parallel = 1.84$, showing that the complex adopts the $(d_{xz}, d_{yz})^4(d_{xy})^1$ ground state. Thus, the EPR results obtained at 4.2 K are fully consistent with the ^{1}H and ^{19}F NMR results obtained in the temperature range 313−173 K.

Comparison of the Electronic Structure. Let us now compare the electronic structure of a series of $[Fe(THFPrP)L_2]^+$ with that of corresponding $[Fe(TPrP)L_2]^+$. The data in Table 1 clearly indicate that the pyrrole-H signal moves downfield on going from $[Fe(THFPrP)L_2]^+$ to $[Fe(TPrP)L_2]^+$ for the same axial ligand, which indicates that the energy gap between the d_π and d_{xy} orbitals, $E(d_\pi) - E(d_{xy})$, decreases in this order. In other words, the population of the electron configurational isomer that adopts the $(d_{xz}, d_{yz})^4(d_{xy})^1$ ground state in eq 4 increases if the meso C_3F_7 groups are replaced by C_3H_7 groups. The difference in electronic structure between $[Fe(THFPrP)L_2]^+$ and $[Fe(TPrP)L_2]^+$ is most explicitly shown in the Curie plots given in Figure 3. While the Curie slopes of the pyrrole-H signals of all the imidazole and pyridine complexes are negative in $[Fe(THFPrP)L_2]^+$ as shown in Figure 3a, some of the complexes such as the 3-MePy and Py complexes exhibit the small positive slopes in $[Fe(TPrP)L_2]^+$. The result indicates that the electronic ground state is switched from $(d_{xy})^2(d_{xz}, d_{yz})^3$ to $(d_{xz}, d_{yz})^4(d_{xy})^1$ as the meso-C_3F_7 groups are replaced by meso-C_3H_7 groups. In the case of the tBuNC complexes, both $[Fe(THFPrP)(^t BuNC)_2]^+$ and $[Fe(TPrP)(^t BuNC)_2]^+$ adopt the $(d_{xz}, d_{yz})^4(d_{xy})^1$ ground state. However, the energy gaps between the d_{xy} and d_π orbitals, $E(d_{xy}) - E(d_\pi)$, determined from the EPR g values at 4.2 K are different: They are −5.0 and −10.7 for $[Fe(THFPrP)(^t BuNC)_2]^+$ and $[Fe(TPrP)(^t BuNC)_2]^+$, respectively, in unit of spin−orbit coupling constant (λ).[67,68] The ruffling of the porphyrin core in $[Fe(THFPrP)L_2]^+$ is presumably larger than that in $[Fe(TPrP)L_2]^+$, because the C_3F_7 group is much bulkier than the C_3H_7 group. In fact, the high barrier to rotation of the 2-MeIm ligand in $[Fe(THFPrP)(2\text{-}MeIm_2)]^+$ as compared with $[Fe(TPrP)(2\text{-}MeIm_2)]^+$ supports the above-mentioned assumption. Thus, the stability of the $(d_{xy})^2(d_{xz}, d_{yz})^3$ ground state in $[Fe(THFPrP)L_2]^+$ relative to $[Fe(TPrP)L_2]^+$ should be ascribed primarily to the electron withdrawing nature of the meso-C_3F_7 group.

(65) Yatsunyk, L. A.; Dawson, A.; Carducci, M. D.; Nichol, G. S.; Walker, F. A. *Inorg. Chem.* **2006**, *45*, 5417–5428.
(66) Ikeue, T.; Yamaguchi, T.; Ohgo, Y.; Nakamura, M. *Chem. Lett.* **2000**, *29*, 342–343.
(67) Palmer, G. Electron Paramagnetic Resonance of Hemoproteins. In *Iron Porphyrins, Part II*; Lever, A. B. P., Gray, H. B., Eds.; Physical Bioinorganic Chemistry Series 2; Addison-Wesley: Reading, MA, 1983; pp 43−88.
(68) Taylor, C. P. S. *Biochim. Biophys. Acta* **1977**, *491*, 137–149.

Conclusion

We have shown on the basis of the ^{1}H NMR, ^{19}F NMR, and EPR results that $[Fe(THFPrP)Py_2]^+$ adopts the $(d_{xy})^2(d_{xz}, d_{yz})^3$ ground state, although the complex was originally reported to be the low-spin complex with the purest $(d_{xz}, d_{yz})^4(d_{xy})^1$ ground state.[43] Comparison of the spectroscopic data between $[Fe(THFPrP)L_2]^+$ and $[Fe(TPrP)L_2]^+$ has revealed that the replacement of the electron donating C_3H_7 by the electron withdrawing C_3F_7 at the meso positions greatly stabilizes the $(d_{xy})^2(d_{xz}, d_{yz})^3$ ground state. On the basis of these results, it is concluded that the less common $(d_{xz}, d_{yz})^4(d_{xy})^1$ ground state is stabilized if one, two, or three of the following conditions are satisfied: (i) axial ligand with low-lying π^* orbitals, (ii) ruffled porphyrin ring, and (iii) electron donating substituent at the meso position.

Acknowledgment. This work was supported by the Grant in Aid (No 22550157) for Scientific Research from Ministry of Education, Culture, Sports, Science and Technology, Japan. Thanks are due to the Research Center for Molecular-Scale Nanoscience, the Institute for Molecular Science (IMS). This work was also supported by Research Center for Materials with Integrated Properties, Toho University, Funabashi, 274-8510, Japan.

Supporting Information Available: Further details are given in Figure S1. This material is available free of charge via the Internet at http://pubs.acs.org.

Abbreviations

Porphyrin Ligands

THFPrP, 5,10,15,20-tetrakis(heptafluoropropyl)-porphyrinato;
OEP, 2,3,7,8,12,13,17,18-octaethylporphyrinato;
TPP, 5,10,15,20-tetraphenylporphyrinato;
F_{20}-TPP, 5,10,15,20-tetrakis(pentafluorophenyl)-porphyrinato;
TArP, 5,10,15,20-tetraarylporphyrinato;
TPrP, 5,10,15,20-tetrapropylporphyrinato;
T^{i}PrP, 5,10,15,20-tetraisopropylporphyrinato;
T^{t}BuP, 5,10,15,20-tetra(*tert*-butyl)porphyrinato;
TRP, 5,10,15,20-tetraalkylporphyrinato;
OETPP, 2,3,7,8,12,13,17,18-octaethyl-5,10,15,20-tetraphenylporphyrinato;
TPrC, 5,10,15,20-tetrapropylchlorinato.

Axial Ligands

HIm, imidazole; 1-MeIm, 1-methylimidazole; 2-MeIm, 2-methylimidazole;
DMAP, 4-(N,N-dimethylamino)pyridine; 4-MePy, 4-methylpyridine;
3-MePy, 3-methylpyridine; 3-ClPy, 3-chloropyridine;
4-CNPy, 4-cyanopyridine;
^{t}BuNC, *tert*-butylisocyanide.